ELSEVIER

Energy and Buildings 27 (1998) 61–68

ENERGY AND BUILDINGS

An urban canyon energy budget model and its application to urban storage heat flux modeling

A. John Arnfield [a,*], C.S.B. Grimmond [b]

[a] *Department of Geography, The Ohio State University, 1036 Derby Hall, Columbus, OH 43210-1361, USA*

[b] *Climate and Meteorology Program, Department of Geography, Indiana University, Bloomington, IN 47405, USA*

Received 19 April 1996; received in revised form 1 May 1997; accepted 1 May 1997

Abstract

To obtain a local-scale urban energy balance by either measurement or modeling it is necessary to determine storage heat flux (ΔQ_s). This flux cannot be measured directly due to the complexity of the urban surface. The Grimmond et al. Objective Hysteresis Model (OHM) [C.S.B. Grimmond, H.A. Cleugh, T.R. Oke, An objective urban heat storage model and its comparison with other schemes, Atmos. Environ., 25B (1991) 311–326] of local-scale ΔQ_s combines empirical equations for individual surface types in the proportion that they are present within the urban area. One surface type for which there is very limited field data is the urban canyon, which consists of the walls of adjacent buildings, the horizontal street-level area separating them (roadways, gardens, parking lots, etc.) and the enclosed air volume. Here the storage heat flux of an urban canyon and the resulting OHM parameters are investigated with a numerical model of a dry urban canyon energy budget. Substrate heat fluxes are derived from simulated surface and substrate temperatures; the latter evolve through time according to the finite difference form of the Fourier heat conduction equation. When compared against measured fluxes, the model performed satisfactorily. Numerical experiments show significant effects on the OHM parameters due to changes in the ratio of building height to separation distance and building wall thermal properties. Effects of intermediate significance were attributable to canyon orientation, wind speed and the timing of the between-building air temperature regime. Air temperature and the timing of the wind speed curve showed only minor significance.

Keywords: Heat transfer; Climate; Simulation; Storage heat flux; Objective hysteresis model; Energy budget hysteresis; Urban building canyon

1. Introduction

Within urban areas, the storage heat flux (ΔQ_s) is, at its most general, the net uptake or release of energy (per unit area and time) by latent and sensible heat changes in the urban canopy air layer and sensible heat changes in buildings, vegetation and the ground. Modeling this energy budget component for urban areas is considerably more challenging than for many other landscape units because of the complex three-dimensional structure of the urban area and the diversity of material types of which the interface is composed. Nevertheless, a knowledge of this term is required in a variety of applications, most notably in synthesizing urban energy budgets and because the thermal inertia provided by this storage term is often regarded as a key process in the genesis of the urban heat island. One recent scheme which offers promise as a means of parameterizing the storage heat flux for city surfaces is the Objective Hysteresis Model (OHM) of Grimmond et al. [1], which has been evaluated independently by Roth and Oke [2].

The OHM characterizes the storage heat flux in terms of the net all-wave radiation Q^* but incorporates the phase difference (i.e., hysteresis) between these energy terms; it may be written as

$$\Delta Q_s = \sum_{i=1}^{n} [a_{1i} Q^* + a_{2i} (\partial Q^* / \partial t) + a_{3i}]$$

in which t is time and the derivative of net radiation is approximated as

$$\partial Q^* / \partial t = 0.5 [Q^*_{t+1} - Q^*_{t-1}]$$

where the derivative is given in W m^{-2} h^{-1} and the energy budget components are evaluated at hourly intervals. The index i identifies a surface type, of which there are n in total.

* Corresponding author: Tel.: +1 614 2927954; fax: +1 614 2926213; e-mail: john.arnfield@osu.edu

PII S0378-7788(97)00026-1

The coefficients a_1, a_2 and a_3 are obtained statistically for each surface type. The parameter a_1 indicates the overall strength of the dependence of the storage heat flux term on net radiation. It will be larger for those surface types for which a greater proportion of the available radiant energy is channeled into subsurface storage. The parameter a_2 describes the degree and direction of the phase relationship between ΔQ_s and Q^*. When a_2 is positive, the net radiation lags behind the ΔQ_s curve on a diurnal basis; when it is negative, the ΔQ_s curve lags the net radiation; when it is zero, no hysteresis is present in the relationship and the two curves are exactly in phase. The parameter a_3 is an intercept term. Grimmond et al. [1] have employed this model for spatially-integrated fluxes ranging in scale from the city block (about 0.5×0.5 km) to an urban land-use zone. Their procedure involves the following steps: (a) a set of coefficients a_1–a_3 is assembled for the different surface types present in the area (b) a survey of the area is conducted to create an inventory of building dimensions and areal coverage of different surface types (c) the coefficients for the OHM model are obtained by weighting those for the individual surface types by the proportion of the total area occupied by each and (d) ΔQ_s is estimated from measured (or estimated) net radiation by summing the contributions of each surface type over all types.

A common surface type in urban areas for which few data are currently available is the urban canyon, which consists of the walls of adjacent buildings, the horizontal street-level area separating them (roadways, gardens, parking lots etc.) and the enclosed air volume. Observational studies of fluxes in urban canyons have been conducted by Nunez and Oke [3], Nakamura and Oke [4], Yoshida et al. [5] and Arnfield and Mills [6]. The OHM model currently relies on data collected over a three day period for a north–south canyon in Vancouver, British Columbia, by Nunez and Oke [3], which give $a_1 = 0.32$, $a_2 = 0.01$ h and $a_3 = -27.7$ W m^{-2}, indicating a surface type for which ΔQ_s is a very significant component of the energy budget but which exhibits very little hysteresis between the storage term and net radiation. The results of Yoshida et al. [5] for an east–west canyon in Kyoto, Japan, suggest similarly small hysteresis ($a_1 = 0.71$, $a_2 = 0.03$ h and $a_3 = -39.7$ W m^{-2}).

The objective of this preliminary study is to use a numerical modeling strategy to investigate the degree to which the OHM coefficients employed for those portions of the urban landscape occupied by canyons can be considered to be universal parameters and, if not, on what site or weather characteristics they might be expected to depend. While the present orientation is towards modeling the response of the urban surface at the *landscape* scale, the procedures outlined may also find applicability in modeling the energy losses and gains of specific facets at the *building* scale. For example, the OHM modeling procedure and coefficients for walls (and roofs) may prove useful in assessing the time-dependence of heating and cooling loads for buildings, or designing building configurations to optimize energy conservation performance.

2. The simulation model

The surface energy budget for a dry, non-vegetated building canyon, is evaluated numerically at multiple points on the canyon floor and walls. This budget is given by

$$K^* + L\downarrow_S + L\downarrow_T - L\uparrow = Q^* = Q_H + Q_G$$

where K^* is the absorbed (or net) solar radiation, $L\downarrow_S$ and $L\downarrow_T$ are the absorbed longwave irradiances from the sky and contributing building facets, respectively, $L\uparrow$ is the emitted longwave irradiance, Q_H is the sensible heat exchange between the facet and the air space between buildings and Q_G is the conductive heat exchange between the facet surface and the interior walls or deep soil beneath the canyon floor.

The absorbed solar and longwave irradiances are computed using the canyon radiation budget model of Arnfield [7,8], with Davies and Hay [9] providing the solar irradiance at the building roof level and its partitioning into direct and diffuse components and Idso [10] giving the longwave counter radiation. The Arnfield model takes into account the geometry of the canyon, its orientation and multiple reflections between the building facets. The emittance $L\uparrow$ is evaluated from the surface temperature and the emissivity of the point on the facet.

The sensible heat exchange is determined from the surface-air temperature difference, using

$$Q_H = h(T_0 - T_a)$$

where T_0 is the surface temperature, T_a is the adjacent air temperature and h is an exchange coefficient, given as a function of between-building wind speed by the equation of Clarke [11].

The conductive flux is evaluated as

$$Q_G = (k_s/\Delta x)(T_0 - T_1)$$

where k_s is the substrate thermal conductivity and T_1 is the temperature at the first subsurface node within the facet fabric, situated at a distance Δx beneath the surface. The temperature T_1, and all other subsurface temperatures within the walls and canyon floor, evolve through time according to the one-dimensional Fourier heat conduction equation. Internal wall temperatures vary throughout the day in response to external forcing and the effects of internal space heating or cooling.

At each time step, T_0 is found numerically by Newton's method. The value of T_0 found depends on the temperature at all other points on the other two facets within the canyon (building walls and/or street-level area), since these determine $L\downarrow_T$. Hence, the temperature field on the canyon surfaces is recomputed after first estimates of T_0 have been determined and this is repeated until the temperature distribution converges.

Once the temperature field has been established, the energy budget terms are evaluated. The budget data presented below are actually those of the last of three simulated days using the same inputs and boundary conditions. The first day permits

the effects of the initial conditions (arbitrary substrate temperature profiles) to dissipate. The second day is used to provide exterior maximum and minimum temperatures and the times of their occurrence, which are used to estimate interior wall temperature regimes.

Finally, the net radiation and substrate heat flux data are averaged by facet and the canyon net radiation and heat storage are evaluated as

$$Q^* = Q_f^* + (H/W)(Q_A^* + Q_B^*)$$

$$\Delta Q_s = Q_{Gf} + (H/W)(Q_{GA} + Q_{GB})$$

where the subscript f denotes the canyon floor mean and the subscripts A and B identify spatial averages over the two walls of the adjacent buildings. H and W are the building height and separation distance, respectively.

The inputs required for the model are as follows: (a) site latitude (b) date (c) building height, separation distance and orientation (d) for each facet, heat capacity, thermal conductivity, albedo and emissivity (e) for the within-canyon air, the temperature and wind speed regimes (f) the lower boundary temperature beneath the canyon floor (g) standard meteorological observations (mean daily air temperature, dew point, barometric pressure, hourly cloud type and amount) and (h) a 'regional' albedo.

It should be noted that the model assumes that the building canyon is long in relation to its cross-sectional dimensions [7] and is dry, so that no latent heat terms enter into the energy budget. In addition, ΔQ_s is considered to consist entirely of conductive heat storage within the building walls and canyon floor. Heat storage within the canyon air itself is neglected.

3. Model evaluation

There exist no published data sets which would provide both the full range of inputs for the simulation model, plus a set of canyon energy budget terms with which the model simulations can be compared. Hence, a rigorous validation test of the model is not possible. Instead, the measured canyon energy budget of Nunez and Oke [3] was compared with a simulation of the same budget, derived by making reasonable interpretations of the weather and site characteristics described in that source.

Table 1 lists the model inputs employed. Building and other canyon geometry characteristics were derived from the authors' descriptions of the site. Wall thermal properties are based on thermal resistance and specific heat data for cinder aggregate concrete blocks (Table 3A in [14]). Canyon floor properties are derived by volume-averaging published specific heat, density and thermal conductivity data for gravel and sandy clay soils [14–16]. Wall albedos were measured by Nunez and Oke [3]. Emissivities are typical values for dry soils and painted surfaces taken from Oke [17]. The diurnal air temperature regime between the buildings was unknown: it is replaced in this model validation experiment with the standard screen-level temperature means for the observation days derived from the Atmospheric Environment Service station at Vancouver International Airport; these data were used for the variable T_a in the equation for Q_H. Wind speeds also were obtained from the airport data but observations were reduced by a 'shelter factor' (0.26) based on a limited amount of simultaneous airport and within-canyon wind speed data given in Nunez and Oke [3]. Mean daily temperature, dew point temperature and station pressure were evaluated from the airport observations. A regional albedo of

Table 1
Input for model evaluation against Nunez and Oke measured data. (Sources for canyon data Nunez and Oke [3,12,13]; see text for other sources)

Study site	Model input		
Location: Vancouver, B.C.	Latitude: 49.3°N		
Canyon Orientation: North–South	Azimuth: 0°		
Measurement period: 9–11 Sept. 1973	10 Sept. 1973		
Regional albedo	0.16		
Mean air temperature	16.8°C		
Mean dew point temperature	13.0°C		
Mean pressure	101.33 kPa		
Incoming longwave radiation	325.5 W $M^{\pm 2}$		
Canyon dimensions and materials	West wall (A)	East wall (B)	Floor
Dimensions	5.59 m	7.91 m	7.54 m
Thickness	0.2 m	0.2 m	0.5 m
Substrate nodes	5@0.040 m apart	5@0.040 m	12@0.038 m
Canyon materials	Concrete	Concrete	Gravel and sandy clay
Heat capacity ($J m^{-3} K^{-1} \times 10^6$)	1.0	1.0	1.4
Thermal conductivity ($W m^{-1} K^{-1}$)	0.67	0.67	0.4
Diffusivity ($m^2 s^{-1} \times 10^{-6}$)	0.67	0.67	0.286
Albedo	0.52	0.62	0.13
Emissivity	0.90	0.90	0.95

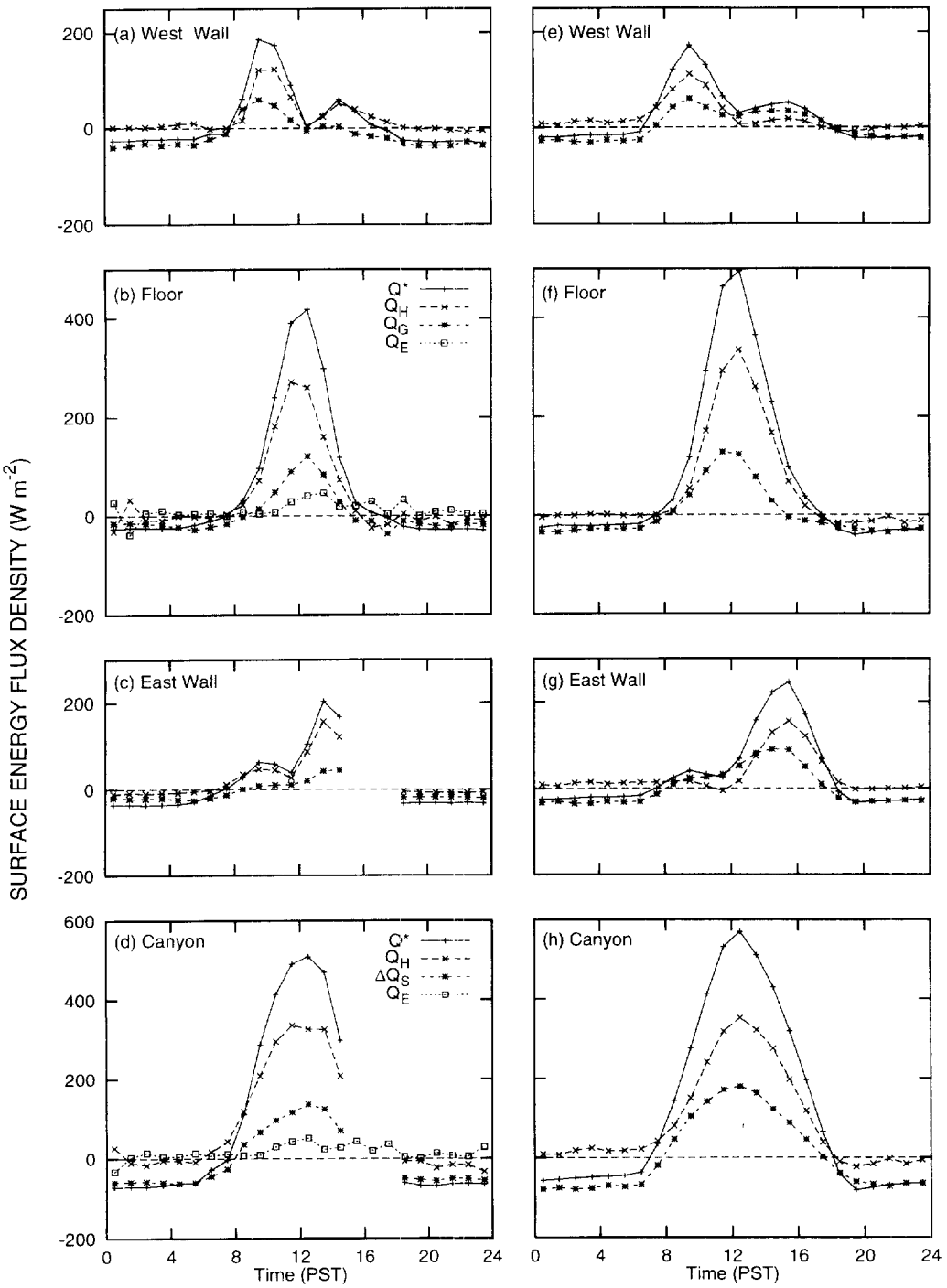

Fig. 1. Panels (a)–(d): measured facet and total canyon energy budgets from Nunez and Oke [3]. Panels (e)–(h): simulated building wall, canyon floor and total canyon energy budgets (for details of simulation, see text).

0.16 is employed to represent a city surface based on published estimates [8,18,19].

In the Nunez and Oke study, the ground surface between the buildings was unpaved and contained some moisture which supported a small but significant latent heat flux. Since the model employed here is for a dry canyon, this term could not be simulated a priori. For model evaluation purposes, however, the measured latent heat fluxes were prescribed so that the other terms in the floor energy budget were responsive to this additional energy sink. (This modification of the model was deleted for the sensitivity studies reported in Section 4, however.)

Fig. 1a–d shows the measured energy budgets for each facet of the canyon and for the canyon system as a whole. Fig. 1e–h shows equivalent data for the canyon simulation. Diurnal patterns of measured and simulated fluxes compare well. West wall data show nighttime sensible heat fluxes near zero with the net radiation and substrate heat fluxes approx-

Table 2
Statistics from comparison of Nunez and Oke data (obs) with modelled data (mod). Units in W m^{-2} except n, m, r, IA and $N\&S$, which are dimensionless

	n	Mean		s.d.		m	c	r^2	RMSE	$RMSE_{sy}$	$RMSE_{usy}$	IA	$N\&S$
		mod	obs	mod	obs								
Q^*													
W	24	22.2	12.7	54.8	60.5	0.84	11.6	0.85	25.0	13.7	20.9	0.95	0.83
F	24	73.9	54.6	162.9	134.6	1.20	8.3	0.99	38.7	33.3	19.6	0.98	0.92
E	21	13.4	11.9	66.0	69.5	0.91	2.6	0.91	20.5	6.6	19.3	0.98	0.91
C	21	104.0	83.4	234.3	216.5	1.08	14.5	0.99	37.3	26.5	26.3	0.99	0.97
Q_H													
W	24	20.4	20.4	30.9	35.8	0.68	6.6	0.62	22.3	11.5	19.1	0.88	0.61
F	24	53.4	39.8	104.9	85.8	1.17	6.6	0.92	35.7	20.2	29.4	0.96	0.83
E	21	17.7	20.6	31.0	46.5	0.52	7.0	0.61	29.5	22.4	19.2	0.84	0.60
C	21	87.4	83.5	127.5	133.0	0.94	9.2	0.96	28.3	9.2	26.8	0.99	0.95
Q_G													
W	24	1.8	−14.2	29.4	28.5	0.90	14.7	0.77	21.6	16.3	14.2	0.87	0.43
F	24	2.8	3.3	49.9	40.4	1.18	−1.1	0.90	17.1	7.1	15.6	0.96	0.82
E	21	−4.3	−6.8	39.9	21.0	1.89	8.6	0.99	19.3	18.8	4.3	0.90	0.16
C(ΔQ_s)	21	0.7	−4.7	97.8	72.0	1.35	7.1	0.99	27.8	25.9	10.1	0.97	0.85

n, number of observations.
s.d., standard deviation.
m, slope, and c, intercept, of linear regression of modelled on observed data.
r^2, coefficient of determination.
RMSE, root mean square error.
$RMSE_{sy}$, systematic part of RMSE.
$RMSE_{usy}$, unsystematic part of RMSE.
IA, index of agreement [20].
$N\&S$, goodness of fit [21].
W: West wall, F: Floor, E: East wall C: Canyon.

imately balancing each other. By day, heat exchange with the air space between the buildings is roughly twice as large as that with the building interior and all components peak during the morning when solar radiation input to an east-facing wall is maximal. A second, smaller peak is apparent during mid-afternoon, driven by reflected solar radiation from the opposite wall. The budget for the east wall is, to a great extent, a 'mirror-image' of that for the west wall. The canyon floor behaves similarly to the walls during the nocturnal hours but, by day, shows a single-peaked set of curves for each component, with the sensible heat flux dissipating a larger fraction of the available net radiation than does conduction to the substrate.

It should be noted that a closer fit between the measured and simulated energy budget terms could probably be achieved by manipulating the magnitudes of the substrate thermal properties, while remaining within the range of values appropriate for the materials described. No justification for such a model 'tuning' could be provided, however.

Table 2 presents comparison statistics for the Nunez and Oke data and the model output. Generally, a satisfactory correspondence was obtained between the simulated and measured energy budgets, given the uncertainties involved in selecting the thermal property and within-canyon meteorological data. The model seems to have captured the essential character of the diurnal regimes and magnitudes of the energy budget components, although there are some apparent differences which remain. The simulated energy budget for the canyon as a whole gives $a_1 = 0.41$, $a_2 = 0.05$ h and $a_3 = -40.0$ W m^{-2}.

4. Numerical experiments

The numerical experiments used to determine the sensitivity of the OHM coefficients a_1–a_3 to model input parameters are conducted as follows: (a) A 'standard' canyon is defined. This is identical to that employed in the previous section to evaluate the performance of the model vs. the Nunez and Oke data, except that the canyon is symmetrical, with building heights and separation distance both equal to 5.59 m. All thermal, radiative and geometrical properties and meteorological data are the same as for the Vancouver, September 9–11 case used above. However, no prescribed latent heat fluxes are incorporated. (b) A single model input (or a related set of model inputs) is varied from the standard case, while holding all other inputs constant. (c) The simulated model Q^* and ΔQ_s data are subjected to the same type of statistical analysis used in Grimmond et al. [1] to yield parameters a_1, a_2 and a_3, both by canyon facet and for the whole system. These experiments are intended to evaluate the degree to which OHM coefficients are dependent on the manipulated variable (or set of variables).

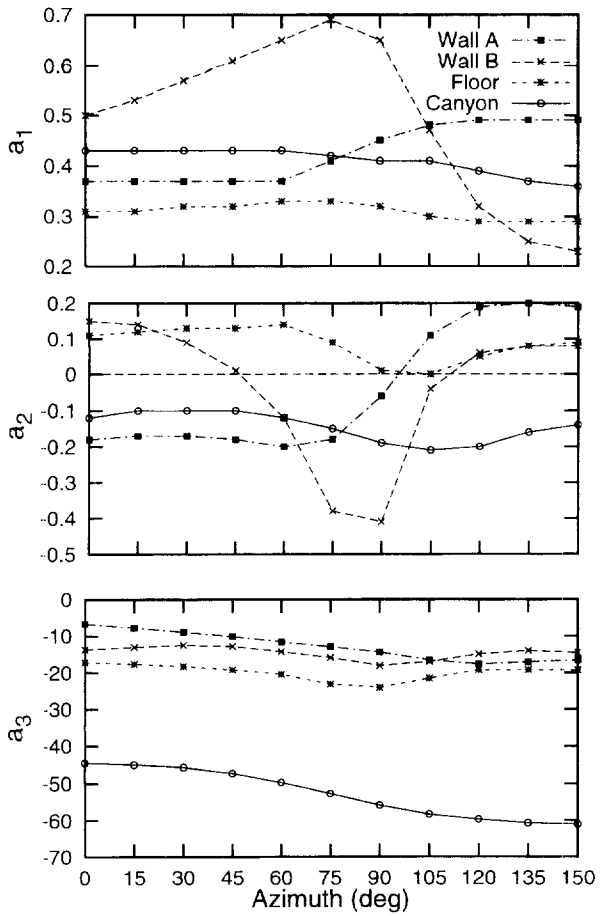

Fig. 2. Simulated OHM coefficients a_1, a_2 and a_3 as determined by canyon orientation.

4.1. Canyon orientation

Fig. 2 shows coefficients a_1–a_3 as a function of canyon orientation angle (i.e., the canyon axis parallel to the building frontage). The standard case is azimuth angle 0°, corresponding to a north–south building wall orientation; wall A is equivalent to the west wall for this case. As the canyon is rotated away from this orientation, coefficients a_1 and a_2 vary markedly for individual facets (especially the walls) as the regime of solar irradiation is changed. However, for the canyon as a whole, the total available net radiation captured in storage decreases only slightly with the rotation. The asymmetry results from the different albedos of the two building walls of the Nunez and Oke canyon, on which the standard case is based (see Table 1). Negative a_2 values suggest that canyon ΔQ_S lags the net radiation and this tendency is most marked at azimuth angles in the range 90°–120° and is least for azimuths from 15° to 45°. The intercept term a_3 decreases by about 15 W m^{-2} as the canyon is rotated by about 180°; again, this asymmetry is primarily an artifact of the differing solar absorptivities of the two walls.

4.2. Canyon aspect ratio

The 'aspect ratio' of a canyon is the ratio of building wall height to building separation distance (H/W). The standard case has an aspect ratio of 1. Table 3 shows that, in general, a larger fraction of the available canyon net radiation is channeled into the storage heat flux when wall height is large in relation to floor width. Furthermore, the greater the aspect ratio, the greater the hysteresis between the two total canyon energy budget components, with hysteresis absent for $H/W=0.5$. Individual canyon facet a_1 and a_2 show similar degrees of dependence on H/W, although both the magnitude and the direction of the hysteresis and the ability of each surface to store energy from the net radiation varies quite widely between the facets. The intercept term becomes less negative with increasing H/W for individual facets but behaves in an opposite manner for the canyon as a whole.

4.3. Within-canyon wind speed

Table 3 shows how the OHM coefficients change when the standard case wind speeds are both halved (row '0.5u') and doubled (row '2u'). As might be expected a_1 decreases as wind speed increases, because intensified air movement increases turbulence and, hence, the effectiveness of the between-building air volume as a heat sink, thus diverting energy from storage within the fabric. A wind speed increase also increases the hysteresis effect (with storage lagging the net radiation) for the canyon as a whole. The intercept term a_3 is little affected by the wind speed within the canyon air volume.

4.4. Within-canyon air temperature

Table 3 illustrates the effect on the OHM model coefficients of changing between-building air temperatures (adding and subtracting 5°C to the standard case data; rows '$T+5$°C' and '$T-5$°C', respectively). These effects are rather small, although lowering the temperature of the canyon air tends to decrease slightly the channelling of heat into storage since it increases the effectiveness of turbulent losses from the facets due to the larger facet surface-air temperature difference. Cooling the canyon air also tends to decrease slightly the hysteresis for the canyon as a whole, with storage lagging the net radiation in all cases. The intercept a_3 is essentially independent of air temperature.

4.5. Within-canyon wind speed phase

It might be expected that the phase characteristics of the within-canyon meteorological data would play a role in determining the phase of the energy budget components and, hence, the OHM coefficients. The wind speed data employed in these model runs is typical of clear uniform airmass conditions, with low values during stable nighttime hours and the highest speeds in the early afternoon, when the atmosphere is most unstable. Table 3 shows the effect of shifting the observed data by 1 h both ways from the standard case. As the peak wind speed is shifted later in the day (row '+1 h'), a_1 decreases very slightly, presumably because the air

Table 3
OHM coefficients from model simulations (coefficient units: a_1, dimensionless; a_2, h; and a_3, W m^{-2}). See text for explanation of modifications to inputs for numerical experiments

	West wall			East wall			Floor			Canyon		
	a_1	a_2	a_3	a_1	a_2	a_3	a_1	a_2	a_3	a_1	a_2	a_3
Canyon aspect ratio: height/width												
2	0.49	−0.33	−6.3	0.59	0.07	−11.8	0.33	0.08	−11.5	0.55	−0.34	−57.6
1	0.37	−0.18	−6.7	0.50	0.15	−13.7	0.31	0.11	−17.2	0.43	−0.13	−44.5
0.5	0.31	−0.09	−6.7	0.46	0.23	−14.7	0.30	0.13	−21.3	0.36	0.00	−36.6
Within canyon wind-speed												
2 u	0.33	−0.22	−5.9	0.46	0.13	−13.0	0.26	0.08	−15.7	0.39	−0.18	−43.5
u	0.37	−0.18	−6.7	0.50	0.15	−13.7	0.31	0.11	−17.2	0.43	−0.13	−44.5
0.5 u	0.42	−0.14	−7.7	0.53	0.17	−14.4	0.34	0.13	−18.0	0.45	−0.08	−45.7
Within canyon air-temperature												
T + 5°C	0.37	−0.19	−7.2	0.50	0.15	−14.0	0.31	0.11	−17.5	0.42	−0.13	−45.6
T	0.37	−0.18	−6.7	0.50	0.15	−13.7	0.31	0.11	−17.2	0.43	−0.13	−44.5
T − 5°C	0.35	−0.14	−9.1	0.47	0.15	−15.1	0.31	0.11	−17.0	0.41	−0.10	−47.2
Within canyon wind speed phase												
− 1 h	0.38	−0.19	−7.1	0.51	0.15	−14.1	0.31	0.11	−17.7	0.43	−0.14	−45.7
0	0.37	−0.18	−6.7	0.50	0.15	−13.7	0.31	0.11	−17.2	0.43	−0.13	−44.5
+ 1 h	0.37	−0.13	−6.3	0.49	0.16	−13.4	0.31	0.12	−17.1	0.42	−0.10	−43.6
Within canyon air temperature phase												
− 1 h	0.46	−0.09	−8.9	0.51	0.22	−14.0	0.32	0.15	−17.8	0.46	0.07	−48.9
0	0.37	−0.18	−6.7	0.50	0.15	−13.7	0.31	0.11	−17.2	0.43	−0.13	−44.5
+ 1 h	0.30	−0.18	−4.9	0.48	0.11	−13.2	0.29	0.07	−16.3	0.38	−0.26	−39.2
Building wall thermal properties (increasing thermal admittance)												
Light	0.23	−0.09	−5.1	0.30	0.11	−9.3	0.31	0.11	−17.2	0.33	−0.02	−37.2
Standard	0.37	−0.18	−6.7	0.50	0.15	−13.7	0.31	0.11	−17.2	0.43	−0.13	−44.5
Heavy	0.57	−0.39	−6.2	0.79	0.14	−17.2	0.31	0.11	−17.1	0.56	−0.36	−50.1

between the buildings becomes a more effective heat sink under high surface temperature conditions, leading to a smaller channelling of heat energy into the building walls and canyon floor. This is true of individual canyon facets and the canyon as a whole.

Shifting the wind speed curve also has a slight effect on the hysteresis coefficient, a_2. Under standard conditions, a_2 is negative, indicating that ΔQ_s lags Q^*. If the wind speeds are altered so that they peak an hour earlier than the standard case (row '− 1 h'), however, a_2 becomes slightly more negative for the total canyon. Physically, this appears to be because permitting peak turbulence to occur earlier in the day enhances Q_H and, hence, decreases ΔQ_s (since Q^* is altered very little), which shifts the peak in the storage heat flux to later in the day, when wind speeds begin to decrease again. This would tend to increase the phase lag between ΔQ_s and Q^* since the storage lags behind the net radiation curve even under standard conditions. By the same argument, shifting the wind speed curve so that the peak occurs later in the afternoon would move the peak in the Q_H curve to later in the day and, hence, move the peak in the ΔQ_s curve to earlier in the day, thus bringing that term and the net radiation more into phase (i.e., a_2 is still negative but is smaller in absolute magnitude).

The intercept term a_3 becomes less negative as the wind speed curve is shifted to later in the day, for the individual facets and for the canyon as a whole. This is a very minor effect, however.

4.6. Within-canyon air temperature phase

Table 3 also shows the sensitivity of the OHM coefficients to a phase shift of ± 1 h in the between-building air temperature curve. The temperature curve has a flat maximum between 1400 h and 1700 h LAT. When the temperature curve is moved 1 h earlier than in the standard case, the high air temperatures occur at a time close to the maximum mean surface temperature, thus suppressing Q_H and enhancing storage of heat within the fabric (i.e., a_1 increases). Shifting the temperature curve to later in the day has the opposite effect.

The phase characteristics of the air temperature curve have a marked effect on the hysteresis coefficient a_2 for the canyon system. When air temperatures peak 1 h earlier than in the standard case, Q_H is suppressed, for reasons explained above. This augments the storage heat flux (as Q^* is only slightly affected by the temperature curve), shifting the ΔQ_s curve peak to an earlier hour. Since ΔQ_s lags the net radiation in the standard case, this reduces the phase difference between the two energy budget components. In fact, a 1 h shift in the air temperature curve to earlier in the day is sufficient to make a_2 slightly positive, indicating that ΔQ_s is leading Q^*. By the same argument, lagging the air temperature curve will

increase the hysteresis between the storage and net radiation terms: in fact, the 1 h shift introduced in this experiment doubles the a_2 coefficient. This phase shift in the temperature curve affects all facets in a similar manner.

The coefficient a_3 becomes less negative as the peak in the air temperature curve becomes later in the day. This is true also for the individual facets.

4.7. Building wall thermal properties

Both the heat capacity (C_s) and thermal conductivity of concrete depend directly on the density of the construction material. The parameter μ_s, defined by

$$\mu_s = \sqrt{k_s C_s}$$

is termed the thermal admittance and is a measure of the degree to which heat may be stored within and withdrawn from the urban fabric. The k_s and C_s values employed in the standard case define an average density concrete for the building walls. Table 3 shows the effect of choosing thermal properties for the concrete walls to give low and high thermal admittance values within the construction concrete range [14]. The values employed in the row labeled 'Light' in Table 3 characterize a low density concrete ($k_s = 0.3$ W m^{-1} K^{-1}; $C_s = 0.6 \times 10^6$ J m^{-3} K^{-1}; $\mu_s = 424$ J s$^{-1/2}$ m^{-2} K^{-1}) while those in the row labeled 'Heavy' are for the high density concrete ($k_s = 1.5$ W m^{-1} K^{-1}; $C_s = 2.1 \times 10^6$ J m^{-3} K^{-1}; $\mu_s = 1775$ J s$^{-1/2}$ m^{-2} K^{-1}). This compares to $\mu_s = 819$ J s$^{-1/2}$ m^{-2} K^{-1} for the standard case. No changes were made in the thermal properties of the canyon floor.

As μ_s increases, a_1 increases for both building walls and for the canyon as a whole as these elements become more receptive to the conduction and storage of heat energy. Likewise, for the west wall and the canyon system in particular, increasing thermal admittance increases the magnitude of the hysteresis as more thermal inertia is introduced into the system. It is noteworthy that, for the low density concrete walls, the hysteresis effect is virtually absent for the canyon data.

The intercept a_3 decreases with increasing μ_s, especially for the east wall and the whole canyon.

5. Conclusions

Although a rigorous validation test of the model on which these results are based was not possible, when the measured energy budget of Nunez and Oke [3] was compared with its simulated counterpart, a satisfactory correspondence was found. The model reproduced overall building canyon behavior well, with some discrepancies in the specific fluxes on some canyon facets. Both the measured data and all subsequent simulations indicate that the storage heat flux is a significant term in the energy disposition of an urban canyon.

Numerical experiments show significant effects on the a_1, a_2 and a_3 parameters due to changes in the aspect ratio of the canyon and building wall thermal properties. Effects of intermediate significance were attributable to canyon orientation, wind speed and the timing of the between-building air temperature regime. Air temperature and the timing of the wind speed curve showed only minor significance.

Empirical data are needed to validate the model. In addition, further work is required to refine the model to incorporate moisture and more realistic arrays of surface materials, to provide a less arbitrary method of parameterizing the sensible heat flux and to explicitly link within-canyon meteorological conditions to their observed boundary-layer equivalents.

Acknowledgements

We would like to thank the Ohio Supercomputer Center for providing computing time and Indiana University for furnishing a Faculty Research Grant for data acquisition.

References

[1] C.S.B. Grimmond, H.A. Cleugh, T.R. Oke, Atmos. Environ. 25B (1991) 311–326.
[2] M. Roth, T.R. Oke, Contributions to Atmos. Phys. 67 (1994) 149–156.
[3] M. Nunez, T.R. Oke, J. Appl. Meteorol. 16 (1977) 11–19.
[4] Y. Nakamura, T.R. Oke, Atmos. Environ. 22 (1988) 2691–2700.
[5] A. Yoshida, K. Tominaga, S. Watatani, Energy and Buildings 15-16 (1991) 417–423.
[6] A.J. Arnfield, G.M. Mills, Int. J. Climatol. 14 (1994) 239–261.
[7] A.J. Arnfield, Numerical modelling of urban surface radiative parameters, in: J.A. Davies (Ed.), Papers in Climatol.: the Cam Allen Memorial Volume, Department of Geography, McMaster Univ. 1976, Discussion Paper, No. 7.
[8] A.J. Arnfield, Phys. Geography 3 (1982) 97–122.
[9] J.A. Davies, J.E. Hay, Calculation of the solar radiation incident on a horizontal surface, in: J.E. Hay, T.K. Won (Eds.), Proceedings of the First Canadian Solar Radiation Data Workshop, 1978, Canadian Atmospheric Environment Service, Toronto, 1980, pp. 32–58.
[10] S.B. Idso, Water Resources Res. 17 (1981) 295–304.
[11] J.A. Clarke, Energy Simulation in Building Design, Adam Hilger, Bristol, 1985.
[12] M. Nunez, T.R. Oke, Boundary-Layer Meteorol. 10 (1976) 121–135.
[13] M. Nunez, T.R. Oke, Geographical Analysis 12 (1980) 373–386.
[14] ASHRAE (American Society of Heating, Refrigerating and Air-Conditioning Engineers), ASHRAE Handbook: 1981 Fundamentals, American Society of Heating, Refrigerating and Air-Conditioning Engineers, Atlanta, 1981.
[15] R.J. List, Smithsonian Meteorological Tables, Smithsonian Institution Press, Washington, 1971.
[16] J.L. Monteith, Principles of Environmental Physics, Elsevier, New York, 1973.
[17] T.R. Oke, Boundary Layer Climates, Methuen, London, 1987.
[18] T.R. Oke, Progress in Phys. Geography 12 (1988) 471–508.
[19] E.C. Kung, R.A. Bryson, D.H. Lenschow, Monthly Weather Rev. 92 (1964) 543–564.
[20] C.J. Willmott, Phys. Geography 2 (1981) 184–194.
[21] J.E. Nash, J.V. Sutcliffe, J. Hydrol. 10 (1970) 282–290.